Journal of Inorganic and General Chemistry
ZAAC
Zeitschrift für anorganische und allgemeine Chemie
DOI: 10.1002/zaac.202000227
ARTICLE

$Li_2Eu_3Br_2[BO_3]_2$: A New Europium(II) Halide Oxoborate with Yellow Luminescence

Jean-Louis Hoslauer,[a] Falk Lissner,[a] Björn Blaschkowski,[a] and Thomas Schleid*[a]

Dedicated to Professor Joachim Maier on the Occasion of his 65th Birthday

Abstract. The europium(II) oxoborate $Li_2Eu_3Br_2[BO_3]_2$ featuring lithium and bromide ions was synthesized by the reaction of Eu_2O_3 with $Li[BH_4]$ as lithium- and boron- as well as $EuBr_3$ as bromide-source at 750 °C for 24 h in silica-jacketed sealed niobium capsules. The yellow, air-stable and yellow fluorescent compound crystallizes in the trigonal space group $R\bar{3}m$ (a = 1049.06(7) pm, c = 2993.1(3) pm, c/a = 2.853, Z = 12). The two crystallographically distinguishable Eu^{2+} cations show either an eightfold coordination as bicapped trigonal prism ($[EuO_6Br_2]^{12-}$) or a ninefold coordination as monocapped square antiprism ($[EuO_5Br_4]^{12-}$). All oxygen atoms stem from isolated triangular $[BO_3]^{3-}$ anions and the Li^+ cations reside in octahedral voids provided by both oxygen atoms and Br^- anions.

Introduction

The chemistry of oxoborates featuring divalent europium shows a great variety of different structural motifs due to various connectivities of the involved oxoborate units in compounds like $Eu_3[BO_3]_2$,[1,2] $Eu_2[B_2O_5]$,[3] or EuB_2O_4.[4] These systems can be further expanded with halide anions, for example, leading to compounds such as $Eu_5F[BO_3]_3$,[5] $Eu_5Cl[BO_3]_3$,[6] $Eu_2ClB_5O_9$, or $Eu_2BrB_5O_9$.[7] If this system is to be further increased, the smallest possible metal cation seems to be Li^+ as most prominent candidate. While lithium-containing oxoborates exist for the structurally and size-related Sr^{2+} cation in compounds like $LiSr[BO_3]$[8] or $LiSr_4[BO_3]_3$,[9] no corresponding Eu^{2+} analogues have been reported yet, although for the trivalent case compounds like $Li_3Eu_2[BO_3]_3$[10] or $Li_6Eu[BO_3]_3$[11] are known in literature. With this contribution we like to add the missing link $Li_2Eu_3Br_2[BO_3]_2$, a pure divalent europium compound, to the collection of these oxoborates.

In oxoborates, the central B^{3+} cation is generally found in three different coordination geometries such as $[BO_4]^{5-}$ tetrahedra, $[BO_3]^{3-}$ triangles and even $[BO_2]^-$ dumbbells in rare examples (e.g. $Gd_4[BO_2]O_5F$[12]). Much like in the case of oxosilicates, these polyhedra often join vertices to form condensed units, like dimers $[B_2O_5]^{4-}$ (e.g. in $Mg_2[B_2O_5]$[13]), six-membered rings $[B_3O_6]^{3-}$ (e.g. in KBO_2[14]) or infinite chains $^1_\infty\{[BO_2]^-\}$ (e.g. in CaB_2O_4), when vertex-linked $[BO_3]^{3-}$ units are concerned. The ability to also form $[BO_4]^{5-}$ tetrahedra further increases the structural diversity to silicate analogues like the *olivine*-type $MgAl[BO_4]$[15] and for these also vertex- (e.g. in χ-$DyBO_3$[16]) and even edge-sharing (e.g. in $Dy_4B_6O_{15}$[17]) can be observed. In case of the above-mentioned europium(II) oxoborates similar structural motifs are found. While in the *ortho*-oxoborate $Eu_3[BO_3]_2$ isolated $[BO_3]^{3-}$ units occur, the *pyro*-oxoborate $Eu_2[B_2O_5]$ contains dimers $[B_2O_5]^{4-}$ with two $[BO_3]^{3-}$ units sharing a vertex. The *meta*-oxoborate EuB_2O_4 exhibits vertex-connected $[BO_3]^{3-}$ units to form one-dimensional chains $^1_\infty\{[BO^v_{2/2}O^t_{2/1}]^-\}$.

Concerning the europium(II) halide oxoborates similar motifs are literature known, like isolated $[BO_3]^{3-}$ units in $Eu_5F[BO_3]_3$,[5] $Eu_5Cl[BO_3]_3$,[6] $Eu_2Cl[BO_3]$, and $Eu_2Br[BO_3]$,[18] with the exceptions of $Eu_2ClB_5O_9$ and $Eu_2BrB_5O_9$,[7] where $[BO_3]^{3-}$ and $[BO_4]^{5-}$ units share vertices to form a three-dimensional network. Hence it is not surprising that in the crystal structure of $Li_2Eu_3Br_2[BO_3]_2$ isolated triangular $[BO_3]^{3-}$ anions can be found as well.

Results and Discussion

The title compound $Li_2Eu_3Br_2[BO_3]_2$ originates from the reaction of Eu_2O_3 with $EuBr_3$ and $Li[BH_4]$ in arc-welded niobium capsules (details in the Experimental Section). It crystallizes trigonally in the space group $R\bar{3}m$ with the lattice parameters a = 1049.06(7) pm and c = 2993.1(3) pm (c/a = 2.853). While no magnetic ordering of the Eu^{2+} cations is observed, the air- and water-stable crystals exhibit a bright yellow fluorescence under ultraviolet light.

In the new oxoborate $Li_2Eu_3Br_2[BO_3]_2$ the $(Eu1)^{2+}$ cations show a bicapped trigonal prism $[EuO_6Br_2]^{12-}$ as coordination environment, while the $(Eu2)^{2+}$ cations are surrounded by nine ligands forming a monocapped square antiprism $[EuO_5Br_4]^{12-}$.

* Prof Dr. Th. Schleid
Fax: +49-711-685-64241
E-Mail: schleid@iac.uni-stuttgart.de
[a] Institute for Inorganic Chemistry
University of Stuttgart
Pfaffenwaldring 55
70569 Stuttgart, Germany

© 2020 The Authors. Zeitschrift für anorganische und allgemeine Chemie published by Wiley-VCH GmbH · This is an open access article under the terms of the Creative Commons Attribution-NonCommercial-NoDerivs License, which permits use and distribution in any medium, provided the original work is properly cited, the use is non-commercial and no modifications or adaptations are made.

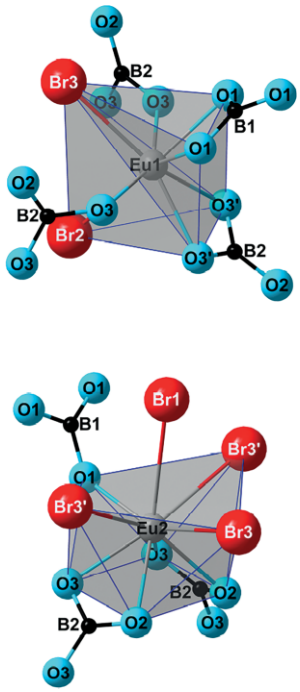

Figure 1. Bicapped trigonal prism $[(Eu1)O_6Br_2]^{12-}$ around $(Eu1)^{2+}$ (top) and monocapped square antiprism $[(Eu2)O_5Br_4]^{12-}$ around $(Eu2)^{2+}$ (bottom) in the crystal structure of $Li_2Eu_3Br_2[BO_3]_2$.

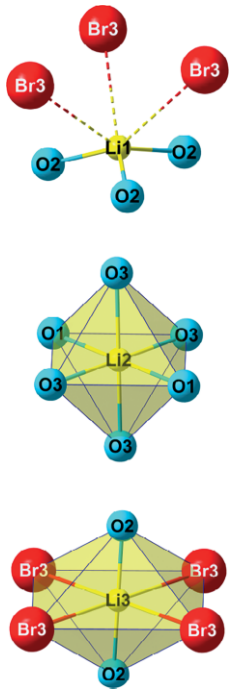

Figure 2. Triangular non-planar $[(Li1)O_3]^{5-}$ unit (top) with three additional Br^- anions forming a trigonal antiprism (or *fac*-octahedron), different enough from the octahedron $[(Li2)O_6]^{11-}$ around $(Li2)^+$ (mid) and the *trans*-octahedron $[(Li3)O_2Br_4]^{7-}$ around $(Li3)^+$ (bottom) in the crystal structure of $Li_2Eu_3Br_2[BO_3]_2$.

Both polyhedra are shown in Figure 1 with their complete oxoborate vicinity consisting of two mono- and bidentate $[BO_3]^{3-}$ ligands each for $(Eu1)^{2+}$, but only one monodentate and two bidentate ones for $(Eu2)^{2+}$. There are three crystallographically distinguishable Li^+ cations in the crystal structure. $(Li1)^+$ forms a triangular non-planar $[(Li1)O_3]^{5-}$ unit. At first glance, if the neighboring Br^- anions are included as well, the coordination sphere is increased as a trigonal antiprism forms. The two remaining Li^+ cations both center more regular octahedra $[(Li2)O_6]^{11-}$ and $[(Li3)O_2Br_4]^{7-}$ as shown in Figure 2. All three Br^- anions are surrounded by six cations forming octahedra ($[(Br1)Eu_6]^{11+}$, $[(Br2)Eu_6]^{11+}$ and $[(Br3)Li_2Eu_4]^{9+}$), where for the latter an additional $(Li1)^+$ ligand must be included due to its rather close proximity as shown in Figure 3. In Figure 4 both distinct oxoborate units $[(B1)O_3]^{3-}$ and $[(B2)O_3]^{3-}$ are presented with their individual cationic and anionic coordination environment added.

The interatomic distances d(Eu–O) = 246–266 pm and d(B–O) = 134–141 pm in $Li_2Eu_3Br_2[BO_3]_2$ are in good agreement with those for $Eu_3[BO_3]_2$ (d(Eu–O) = 235–296 pm, d(B–O) = 136 pm), whereas them for d(Eu···B) = 294–301 pm appear much shorter than in $Eu_3[BO_3]_2$ (d(Eu···B) = 316–330 pm).[1] The interatomic distances d(Eu–Br) = 303–329 pm in $Li_2Eu_3Br_2[BO_3]_2$ resemble very much the average distances d(Eu–Br) = 309–328 pm found in $SrBr_2$-type $EuBr_2$[19,20]

While the distances d(Li1–Br3) = 326 pm and d(Li3–Br3) = 299 pm are much larger than d(Li–Br) = 275 pm in rocksalt-type LiBr,[21] most distances d(Li–O) = 197–223 pm are relatively close to those of 200 pm in *anti*-fluorite-type Li_2O.[22]

In view of the lithium coordination spheres (Figure 2 and Table 4), the rather incomplete polyhedron of $(Li1)^+$ deserves some comment. With the help of ECoN calculations (ECoN = Effective Coordination Number according to Hoppe[23]) using the ionic radii $r_i(Li^+)$ = 76 pm, $r_i(O^{2-})$ = 140 pm, and $r_i(Br^-)$ = 196 pm (all for C.N. = 6),[24] all oxide anions show contributions such as 0.89 to 1.28 to ECoN(Li1) = 3.14, ECoN(Li2) = 5.91 and ECoN(Li3) = 4.61. For ECoN(Li2), there is no other contribution, so 1.16 (2×) from O1 and 0.89 (4×) from O3 yields the highest ECoN value for all lithium cations in $Li_2Eu_3Br_2[BO_3]_2$. The mixed-anion coordination spheres of Li1 and Li3 cause very different results, however. While Li3 exhibits with 1.28 (2×) from O2 and 0.36 (4×) from Br3 a reasonably high number of almost 5, Li1 settles with just a little more than 3 as sum of 1.03 (3×) from O2 and 0.02 (3×) from Br3. So the special function of $(Br3)^-$ to fulfill as only bromide anion in $Li_2Eu_3Br_2[BO_3]_2$ the coordination demand of both lithium cations (Li1 and Li3) with mixed-anion spheres seems to be demanding.

The $[BO_3]^{3-}$ anions are highly symmetric when centered with B1 (d(B1–O) = 137 pm (3×); angle O1–B1–O1 = 120°, d(B1–Δ) = 5 pm), but show a remarkable bond length variation for B2 (d(B2–O) = 133 pm (1×) + 142 pm (2×); angle O1–B2–O1 = 114–123°, d(B2–Δ) = 4 pm). Reason might be the bidentate grip at the $(Eu1)^{2+}$ cations, which mainly works via O3···O3 (Figure 1).

The possibility of the formula $Li_2Eu_3Br_2[BO_3]_2$ being composited from 2×LiBr[21] and $Eu_3[BO_3]_2$,[1,2] might inspire some number games. So the molar volume of V_m = 143.18 $cm^3 \cdot mol^{-1}$ of the first one is not so well reflected by the sum V_m = 139.92 $cm^3 \cdot mol^{-1}$ of the latter two according to

© 2020 The Authors. Zeitschrift für anorganische und allgemeine Chemie published by Wiley-VCH GmbH

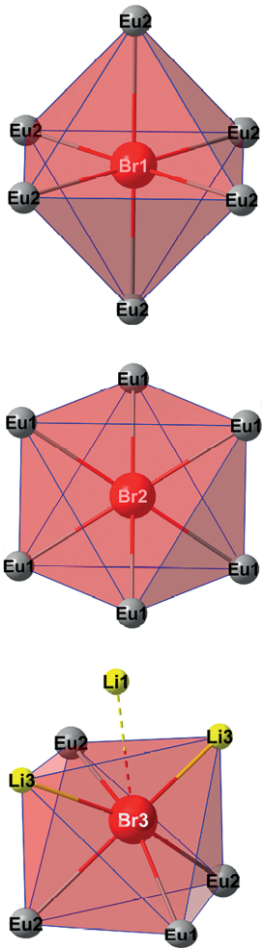

Figure 3. Octahedra $[(Br1)Eu_6]^{11+}$ (top), $[(Br2)Eu_6]^{11+}$ (mid) and $[(Br3)Li_2Eu_4]^{9+}$ (bottom) with an additional $(Li1)^+$ ligand indicated by a dotted bond in the crystal structure of $Li_2Eu_3Br_2[BO_3]_2$.

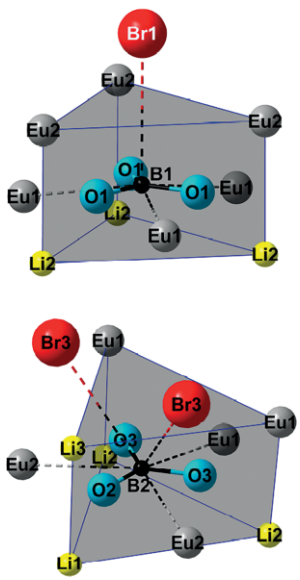

Figure 4. Cationic and anionic coordination environment of the isolated triangular $[(B1)O_3]^{3-}$ (top) and $[(B2)O_3]^{3-}$ units (bottom) in the crystal structure of $Li_2Eu_3Br_2[BO_3]_2$.

$2 \times 25.13\ cm^3 \cdot mol^{-1} + 89.66\ cm^3 \cdot mol^{-1}$ ($\Delta = 2.3\,\%$), suggesting $Li_2Eu_3Br_2[BO_3]_2$ to be less dense than the sum of its components. On the other hand the comparison of their Madelung Part of the Lattice Energy (MAPLE according to Hoppe[25,26]) reveals a much better fit, when $MAPLE(Li_2Eu_3Br_2[BO_3]_2) = 35{,}377\ kJ \cdot mol^{-1}$ is juxtaposed to the MAPLE sum ($35{,}195\ kJ \cdot mol^{-1}$) resulting from the components according to $2 \times MAPLE(LiBr) = 2 \times 882\ kJ \cdot mol^{-1} + MAPLE(Eu_3[BO_3]_2) = 33{,}431\ kJ \cdot mol^{-1}$ ($\Delta = 0.5\,\%$).

While the crystal structure of the europium(II) *ortho*-oxoborate $Eu_3[BO_3]_2$,[1,2] can be described isostructurally to $Ca_3[BO_3]_2$[27] as an *anti*-corundum-type arrangement derived from a hexagonal close packing of Eu^{2+} cations with $[BO_3]^{3-}$ units occupying $^2/_3$ of the octahedral voids in every layer, similarly, the crystal structure of $Li_2Eu_3Br_2[BO_3]_2$ might be understood as being based on a cubic close packing of Eu1, Eu2, Li3 and Br1 (Figure 5). Herein Eu1 and Eu2 form separate layers, in the following description labeled with the letters A, B and C, while Li3 and Br1 form layers with mixed occupation further labeled with A′, B′ and C′ and stacked along [001]. With a stacking order of A′BCABC′ABCAB′CABCA′ it can be seen that the mixed Li3 and Br1 layers are separated by four europium layers, where two Eu2 layers sandwich a Eu1 double layer. In this packing motif, the octahedral voids are filled in repeating patterns, which can be described as layers consisting of two kinds of ions. Here, every second row and column will feature the same ions, while in every other row and column the two ions alternate as shown in Figure 6.

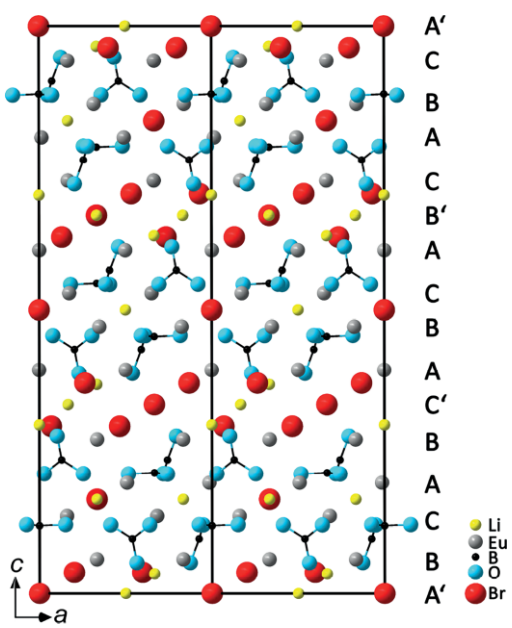

Figure 5. Two unit cells of $Li_2Eu_3Br_2[BO_3]_2$ as viewed along [110] emphasizing the cubic close packing motif along [001] (labeled with ABC and A'B'C'). The $[BO_3]^{3-}$ triangles are drawn with their molecular bonds for easier recognition.

This motif is found for the octahedral voids between the Eu2 and the mixed Li3 and Br1 layers with Li1 and Br3 filling the voids, and between the two Eu1 layers with Li2 and Br2 filling the voids. The missing oxoborate units $[BO_3]^{3-}$ reside

© 2020 The Authors. Zeitschrift für anorganische und allgemeine Chemie published by Wiley-VCH GmbH

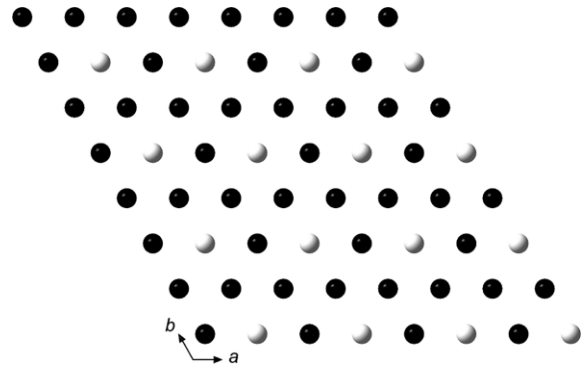

Figure 6. Structural motif for the cation and anion layers filling the octahedral voids in the crystal structure of $Li_2Eu_3Br_2[BO_3]_2$. The black and white color coding does not refer to a specific ion, but is used to distinguish the two different kinds of ions.

in tetrahedral voids between the Eu1 and Eu2 layers. While in the europium(II) *ortho*-oxoborate $Eu_3[BO_3]_2$ the $[BO_3]^{3-}$ triangles arrange normal to the [001] direction, $Li_2Eu_3Br_2[BO_3]_2$ also features triangles in an approximate angle of 70° relative to the *c* axis (Figure 5). Crystallographic data and structure refinement results are summarized in Table 1, atom positions and anisotropic displacement parameters are listed in Table 2 and Table 3, respectively, and selected interatomic distances are given in Table 4.

Table 1. Crystallographic data for $Li_2Eu_3Br_2[BO_3]_2$ and their determination.

	$Li_2Eu_3Br_2[BO_3]_2$
Crystal system	trigonal
Space group	$R\bar{3}m$ (no. 166)
a /pm	1049.06(7)
c /pm	2993.1(3)
c/*a*	2.853
Formula units, *Z*	12
Calculated density, D_x /g·cm^{-3}	5.219
Molar volume, V_m /cm^3·mol^{-1}	143.12
Instrument	STOE STADIVARI
Radiation	Mo-K_α, λ = 71.07 pm
F(000)	3876
Range, $\pm h$ / $\pm k$ / $\pm l$	13 / 13 / 38
$2\Theta_{max}$ /°	54.65
Absorption coefficient, μ /mm^{-1}	27.94
Data corrections	Lorentz and polarization correction using X-Area [28], absorption correction using STOE LANA [29]
Number of measured vs. symmetrically independent reflections	6451 / 796
R_{int} / R_σ	0.061 / 0.038
Structure solution and refinement	SHELXS-97 [30, 31], SHELXL-97 [32, 33]
R_1 for *n* reflections with $\|F_o\| \geq 4\sigma(F_o)$	0.040 (*n* = 622)
R_1 / wR_2 for all reflections	0.056 / 0.096
Goodness of fit (Goof)	1.009
Extinction coefficient, *g*	0.00002(1)
Residual electron density, $\rho_{max/min}$ / e$^-$·Å^{-3}	1.91 / –1.84

Energy-dispersive X-ray Spectroscopy (EDXS)

To identify possible contaminations with for example niobium from the metal capsule an EDX spectrum was taken (Figure 7). Therefore, several yellow single crystals of $Li_2Eu_3Br_2[BO_3]_2$ were selected to guarantee a uniform composition. Due to the measuring method, neither lithium nor boron could be determined. The carbon signal is due to the sample sputtering with graphite to increase the conductivity, the silicon signal is likely a silicon escape peak from the detector. Although no quantitative results could be taken from the EDXS analysis, it becomes evident that the compound features europium and bromine and does not show any niobium from the growth on the niobium capsule walls.

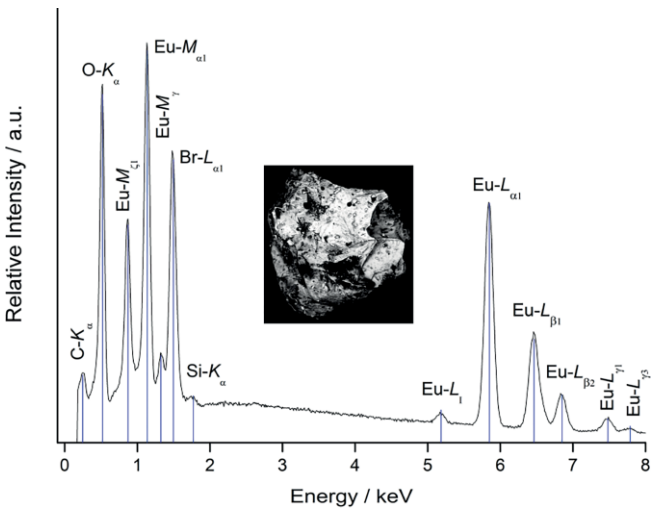

Figure 7. EDX spectrum of $Li_2Eu_3Br_2[BO_3]_2$ (V_{acc} = 15 kV) with characteristic element lines labeled.

Magnetic Properties

As $Li_2Eu_3Br_2[BO_3]_2$ features two different Eu^{2+} cations, but three in the empirical formula, which due to their $4f^7$ configuration often show magnetic ordering, the magnetic behavior was tested. For this measurement 15 mg of $Li_2Eu_3Br_2[BO_3]_2$ were filled into a tared gelatin capsule, whose magnetic moment was determined before. It was then placed into a SQUID magnetometer (Quantum Design, San Diego) and measured in a temperature interval from 2 K up to 300 K at a magnetic field strength of 100 Oe. From this data, the inverse molar susceptibility χ_{mol} was determined (Figure 8).

Figure 8 shows a typical paramagnetic behavior as the inverse molar susceptibility increases linearly with the temperature. The determined magnetic moment of Eu^{2+} (μ_{eff} = 7.64 ± 0.02 μ_B) for the Eu^{2+} cations found in close approximation to the theoretical Russel-Saunders magnetic moment of 7.94 μ_B for an isolated Eu^{2+} cation ($^8S_{7/2}$):

$$\mu_{eff} = g \cdot \sqrt{S \cdot (S+1)}\ \mu_B = 7.94\ \mu_B$$

The nearly double zero-crossing of the χ_m^{-1} vs. *T* curve does not leave any evidence for magnetic ordering phenomena, which does surprise as the shortest $Eu^{2+}\cdots Eu^{2+}$ distances of

© 2020 The Authors. Zeitschrift für anorganische und allgemeine Chemie published by Wiley-VCH GmbH

Table 2. Fractional atomic coordinates, Wyckoff positions, and equivalent isotropic displacement parameters for $Li_2Eu_3Br_2[BO_3]_2$.

Atom	Site	x/a	y/b	z/c	U_{eq} /pm^2
Li1	6*c*	0	0	0.2977(18)	295(124)
Li2	9*d*	$^1/_2$	0	$^1/_2$	240(91)
Li3	9*e*	$^1/_2$	0	0	185(85)
Eu1	18*h*	0.15912(4)	–*x*/*a*	0.13726(3)	127(3)
Eu2	18*h*	0.16612(4)	–*x*/*a*	0.93889(3)	145(3)
Br1	3*a*	0	0	0	359(11)
Br2	3*b*	0	0	$^1/_2$	260(9)
Br3	18*h*	0.13204(9)	–*x*/*a*	0.62863(7)	278(4)
B1	6*c*	0	0	0.1204(9)	81(52)
B2	18*h*	0.2044(9)	–*x*/*a*	0.4303(7)	215(40)
O1	18*h*	0.0752(5)	–*x*/*a*	0.8778(3)	178(23)
O2	18*h*	0.1032(5)	–*x*/*a*	0.2781(3)	153(21)
O3	36*i*	0.4127(7)	0.3609(7)	0.1217(2)	165(15)

Table 3. Anisotropic displacement parameters (U_{ij} /pm^2) [a] for $Li_2Eu_3Br_2[BO_3]_2$.

Atom	U_{11}	U_{22}	U_{33}	U_{12}	U_{13}	U_{23}
Li1	191(148)	U_{11}	501(348)	$^1/_2$ U_{11}	0	0
Li2	211(143)	232(198)	285(230)	$^1/_2$ U_{22}	$^1/_2$ U_{23}	94(168)
Li3	154(122)	322(216)	134(188)	$^1/_2$ U_{22}	$^1/_2$ U_{23}	–141(156)
Eu1	91(3)	U_{11}	185(5)	33(3)	–U_{23}	4(2)
Eu2	132(3)	U_{11}	180(5)	73(3)	–U_{23}	9(2)
Br1	284(13)	U_{11}	509(30)	$^1/_2$ U_{11}	0	0
Br2	180(11)	U_{11}	420(26)	$^1/_2$ U_{11}	0	0
Br3	284(6)	U_{11}	221(9)	109(7)	–U_{23}	–5(4)
B1	91(75)	U_{11}	60(128)	$^1/_2$ U_{11}	0	0
B2	128(57)	U_{11}	394(114)	68(72)	–U_{23}	28(39)
O1	58(29)	U_{11}	337(64)	–32(37)	–U_{23}	4(25)
O2	162(35)	U_{11}	131(50)	79(41)	–U_{23}	–36(22)
O3	120(33)	147(35)	200(38)	45(28)	–4(31)	36(30)

a) $U_{eq} = {}^1/_3\,[U_{33} + {}^4/_3(U_{11} + U_{22} - U_{12})]$[34].

Table 4. Selected interatomic distances (*d* /pm) for $Li_2Eu_3Br_2[BO_3]_2$.

Li1–O2	(3×)	196.5	Eu1–Br3	(1×)	306.7
Li1···Br3	(3×)	325.9	Eu1–O3	(2×)	251.1
Li2–O1	(2×)	212.9	Eu1–O3’	(2×)	254.5
Li2–O3	(4×)	222.7	Eu1–O1	(2×)	254.5
Li3–O2	(2×)	201.6	Eu1–Br2	(1×)	328.6
Li3–Br3	(4×)	299.3	Eu2–Br3	(1×)	303.6
			Eu2–O1	(1×)	246.4
B1–O1	(3×)	136.7	Eu2–O3	(2×)	254.0
B2–O2	(1×)	133.4	Eu2–O2	(2×)	266.1
B2–O3	(2×)	141.6	Eu2–Br3’	(2×)	345.3
			Eu2–Br1	(1×)	352.9

362 and 373 pm are in close approximation to those in the ferromagnetic $Eu_3[BO_3]_2$ (d(Eu···Eu) = 359 pm)[2] and in ferromagnetic EuO (d(Eu···Eu) = 363 pm).[35]

Color and Luminescence

The new europium(II) oxoborate $Li_2Eu_3Br_2[BO_3]_2$ shows a yellow color as bulk material, very much like the other europium(II) oxoborates ($Eu_3[BO_3]_2$, $Eu_2[B_2O_5]$ and EuB_2O_4) and halide oxoborates ($Eu_2ClB_5O_9$ and $Eu_2BrB_5O_9$) mentioned before. Under ultraviolet light (λ = 254 nm), however $Li_2Eu_3Br_2[BO_3]_2$ and $Eu_3[BO_3]_2$ have some different behavior. Crystals of $Eu_3[BO_3]_2$[1,2] were obtained in another experiment and can therefore be used for comparison with the title compound. Although both compounds do not differ much in body color, their luminescence is different with $Eu_3[BO_3]_2$ glowing red and $Li_2Eu_3Br_2[BO_3]_2$ showing a bright yellow luminescence under ultraviolet light (λ = 254 nm, MinUVIS Desaga, Nümbrecht) as shown in Figure 9 and Figure 10.

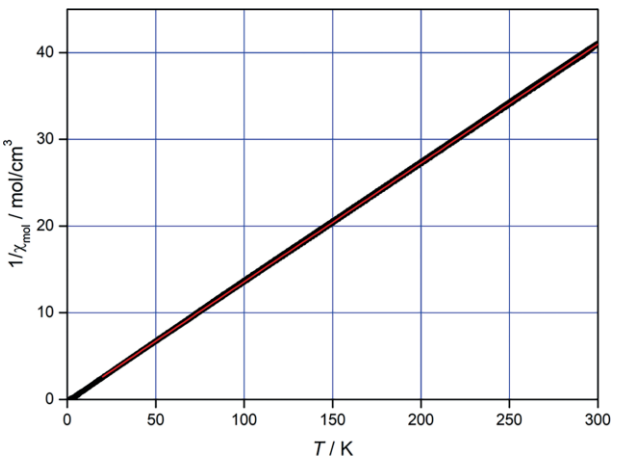

Figure 8. Inverse molar susceptibility of $Li_2Eu_3Br_2[BO_3]_2$ after subtraction of all temperature-independent components. A linear fit (red line) was used to determine the magnetic moment for the Eu^{2+} cations according to the Curie-Weiss law.

While the pure europium(II) *ortho*-oxoborate $Eu_3[BO_3]_2$ exhibits red fluorescence, the hypsochromic shift of the title

© 2020 The Authors. Zeitschrift für anorganische und allgemeine Chemie published by Wiley-VCH GmbH

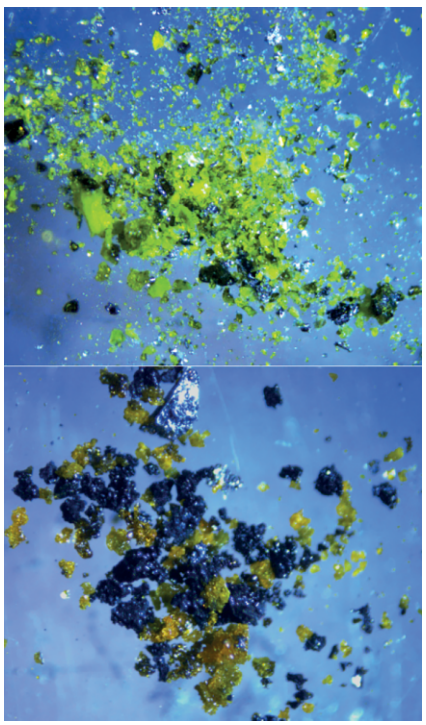

Figure 9. Crystals of $Li_2Eu_3Br_2[BO_3]_2$ (top) and $Eu_3[BO_3]_2$ (bottom) under a light microscope. While $Li_2Eu_3Br_2[BO_3]_2$ shows a bright lemon-yellow color, $Eu_3[BO_3]_2$ is orange-yellow. The black side-phases are mixtures of niobium metal pieces, as the used capsules become extremely brittle, and unknown niobium-rich phases according to EDXS determinations.

Figure 10. Luminescence of $Li_2Eu_3Br_2[BO_3]_2$ (top) and $Eu_3[BO_3]_2$ (bottom) under UV light (λ = 254 nm).

compound $Li_2Eu_3Br_2[BO_3]_2$ may also originate from the introduction of bromide anions into the system. If other europium(II) bromides and oxide bromides are used for comparison, such as $EuBr_2$[36] or Eu_4OBr_6,[37] a blue fluorescence is observed. The same effect is found for $Sr_3[BO_3]_2$ that shows a yellow fluorescence,[38] when doped with Eu^{2+}, in comparison to Eu^{2+}-doped $SrBr_2$, which exhibits a blue emission.[39] Another surprising difference emerges, when the luminescence of $Li_2Eu_3Br_2[BO_3]_2$ is further compared with the performance of other europium(II) oxoborates and their halide derivatives (Table 5).

Table 5. Selected europium(II) oxoborates, halide oxoborates and $Eu_2[SiO]_4$ with their reported body colors and their emission maxima of luminescence.

Composition	Body color	Luminescence (λ_{max} /nm)
$Eu_2[SiO]_4$	yellow [40]	578 nm [40]
$Eu_3[BO_3]_2$	yellow [2]	orange red
EuB_2O_4	yellow [41]	370 nm [42]
EuB_4O_7	gray [41]	372 nm [42]
$Eu_2[B_2O_5]$	yellow [41]	–
$Eu_2Cl[BO_3]$	black [18] a)	–
$Eu_2Br[BO_3]$	black [18] a)	–
$Eu_2ClB_5O_9$	yellow [43]	430 nm [43]
$Eu_2BrB_5O_9$	yellow [43]	435 nm [43]
$Eu_5F[BO_3]_3$	yellow [5]	418 nm [5]
$Eu_5Cl[BO_3]_3$	orange red [6]	–

a) Most probably mixed-valent europium halide oxoborates according to $Eu_6X[BO_3]_4$ (X = Cl and Br)[44].

Although the reported body colors show mostly similar yellow shades, the corresponding emission maxima range in the region from 370 to 440 nm. The only exception seems to be the above shown europium(II) *ortho*-oxoborate $Eu_3[BO_3]_2$ (Figure 10). This does not surprise, as europium(II) compounds show a high dependency in their emission wavelengths of the surrounding coordination environment due to energetically close 5d and 4f orbitals thus leading to 5d–4f emissions.[43] Additionally, the yellow body color and emission of $Li_2Eu_3Br_2[BO_3]_2$ also reminds of the optically similar europium(II) *ortho*-oxosilicate $Eu_2[SiO_4]$.[40] As the luminescent properties of the latter have been subject to careful investigations by members of our group, similar studies are planned in collaboration with experts in this field for a future publication, since properties like emission maxima of bulk luminescence and the necessary theoretical considerations are beyond the scope of this article.

Conclusion and Outlook

The yellow multinary europium(II) *ortho*-oxoborate $Li_2Eu_3Br_2[BO_3]_2$ can be obtained from Eu_2O_3, $EuBr_3$ and $Li[BH_4]$ as reducing agent in niobium capsules. Its yellow body color is repeated by its luminescence, which surprises, since both crystallographically independent Eu^{2+} cations show mixed-anionic coordination spheres with oxide and bromide anions. Several attempts have been made to also prepare the other lithium-halide derivatives $Li_2Eu_3Cl_2[BO_3]_2$ and $Li_2Eu_3I_2[BO_3]_2$, but none of these products were formed. In the future, the possible formation of calcium, strontium and barium as well as potential ytterbium(II) analogues should be

© 2020 The Authors. Zeitschrift für anorganische und allgemeine Chemie published by Wiley-VCH GmbH

tested. The stoichiometry must be adjusted to minimize the amount of side-products. The luminescence properties of $Li_2Eu_3Br_2[BO_3]_2$ and $Eu_3[BO_3]_2$ have to be measured in more detail and interpreted to understand the strong red-shift for the pure *ortho*-oxoborate. The thermal behavior of the title compound under air and inert conditions should be followed by differential scanning calorimetry (DSC), differential thermal analysis (DTA) and powder diffraction to check for possible conversions or phase transitions. Finally, a possible Li^+-cation conductivity could be investigated, which might be realized by lithium-containing channels parallel to [100], [110], and [001]. Although the shortest distances along these channels *d*(Li2···Li2) and *d*(Li3···Li3) = 524 pm may be problematic for Li^+-cation conductivity, the distances *d*(Li1···Li2) = 496 pm and *d*(Li1···Li3) = 321 pm should open a path for lithium-ion conductivity, in particular for $(Li1)^+$ with its very anisotropic displacement parameters (Table 3).

Experimental Section

$Li_2Eu_3Br_2[BO_3]_2$ was formed in high yield during an attempt to use $Li[BH_4]$ as reducing agent to obtain europium(II) oxide halides and potential hydrides. A previous experiment has revealed that europium(II) hydride chloride EuHCl could be prepared among other side-products from Eu_2O_3 and LiCl using $Li[AlH_4]$ as reducing agent.[45] When $Li[BH_4]$ and $EuBr_3$ were used, no red EuHBr formed, but $Li_2Eu_3Br_2[BO_3]_2$. For both reactions, however, the reducing power of $Li[AlH_4]$ and $Li[BH_4]$ was obviously strong enough to generate divalent europium compounds exclusively, whereas borothermic reductions with elemental boron in the presence of halide anions often results in the formation of mixed-valent europium compounds, such as $Eu_6Cl[BO_3]_4$ and $Eu_6Br[BO_3]_4$[44] according to $(Eu^{2+})_5(Eu^{3+})(X^-)([BO_3]^{3-})_4$ (X = Cl and Br). The bright yellow and air-stable platelets of $Li_2Eu_3Br_2[BO_3]_2$ were prepared from europium sesquioxide (Eu_2O_3: 99.99 %, ChemPur, Karlsruhe), europium tribromide ($EuBr_3$: 99.99 %, Alfa Aesar, Karlsruhe) and lithium tetrahydroborate ($Li[BH_4]$: 95 %, Acros Organics, Nidderau). For this reason Eu_2O_3 (88 mg, 0.25 mmol, 1 equiv.) was mixed with $EuBr_3$ (98 mg, 0.25 mmol, 1 equiv.) as well as $Li[BH_4]$ (16 mg, 0.75 mmol, 3 equiv.) and filled into a niobium capsule (5 cm × 1 cm diameter, 1 mm wall thickness), made from niobium metal-pipes (Holdenrieder, Bergkirchen). The pipes were cut into 5 cm long pieces and closed on one side using an inert-gas arc-welder. The ampoule was loaded inside an argon-filled glove box (MEGA GS Glovebox Systemtechnik, Malsch) and sealed by arc-welding in helium environment at 800 mbar. As niobium reacts with oxygen and nitrogen at elevated temperatures, the capsules were further jacketed with an evacuated fused silica ampoule and heated in a muffle furnace (Nabertherm L9/12, Liliental) for 24 h at 750 °C with a heating rate of 60 $K \cdot h^{-1}$ and a cooling rate of 15 $K \cdot h^{-1}$. The capsules were then opened in an argon-filled glove box again. The product consisted of a black powder with unknown composition together with bright yellow, air-stable crystals forming at the capsule walls. A following EDXS analysis (SX 100, Cameca, Paris) showed no traces of niobium in the new compound, while a high niobium concentration could be detected in the black side-product. The experiment was successfully repeated two times, although no phase-pure product could yet be generated. A single crystal was chosen for single-crystal X-ray diffraction experiments (Stadivari, Stoe & Cie, Darmstadt) and the crystal structure was determined.

Acknowledgements

Open access funding enabled and organized by Projekt DEAL.

Keywords: Bromides; Lithium; Europium; Oxoborates; Luminescence

References

[1] K. I. Machida, G. Y. Adachi, H. Hata, J. Shiokawa, *Bull. Chem. Soc. Jpn.* **1981**, *54*, 1052–1055.
[2] O. Reckeweg, Ch. Funk, F. J. DiSalvo, Th. Schleid, *Z. Anorg. Allg. Chem.* **2016**, *642*, 1051–1051.
[3] Ch. Funk, Th. Schleid, *Z. Kristallogr.* **2018**, *S38*, 97–98.
[4] K. Machida, G. Y. Adachi, J. Shiokawa, *Acta Crystallogr., Sect. B* **1979**, *35*, 149–151.
[5] F. K. Kazmierczak, H. A. Höppe, *Eur. J. Inorg. Chem.* **2010**, *18*, 2678–2681.
[6] O. Reckeweg, A. Schulz, F. J. DiSalvo, *Z. Naturforsch. B* **2016**, *66*, 359–365.
[7] A. Levasseur, C. Fouassier, *Compt. Rend. Seanc. Acad. Sci. C* **1971**, *272*, 80–82.
[8] W.-D. Cheng, H. Zhang, Q.-S. Lin, F.-K. Zheng, J.-T. Chen, *Chem. Mater.* **2001**, *13*, 1841–1847.
[9] L. Wu, X.-L. Chen, H. Li, M. He, Y.-P. Xu, X.-Z. Li, *Inorg. Chem.* **2005**, *44*, 6409–6414.
[10] G. K. Abdullaev, Kh. S. Mamedov, G. G. Dzhafarov, *Azerb. Khim. Zh.* **1977**, 115–119.
[11] F. W. Tan, C. Fouassier, P. Hagenmuller, *J. Phys. Chem. Sol.* **1987**, *48*, 245–248.
[12] H. A. Höppe, *Z. Naturforsch. B* **2015**, *70*, 769–774.
[13] Y. Takéuchi, *Acta Crystallogr.* **1952**, *5*, 574–581.
[14] W. H. Zachariasen, *J. Chem. Phys.* **1937**, *5*, 919–922.
[15] W. Kleber, H.-J. Bautsch, J. Bohm, D. Klimm, *Einführung in die Kristallographie*, 19. Auflage, Oldenbourg-Verlag, München, **2010**.
[16] H. Huppertz, B. von der Eltz, R.-D. Hoffmann, H. Piotrowski, *J. Solid State Chem.* **2002**, *166*, 203-212.
[17] H. Huppertz, B. von der Eltz, *J. Am. Chem. Soc.* **2002**, *124*, 9376–9377.
[18] K. Machida, G. Adachi, J. Shiokawa, *Chem. Lett.* **1982**, *11*, 41–44.
[19] H. P. Beck, *Doctoral* Thesis, University of Karlsruhe, **1972**.
[20] J. P. Sanchez, J. M. Fried, H. Bärnighausen, A. J. van Duyneveldt, *Inorg. Chem.* **1985**, *24*, 408–415.
[21] H. Ott, *Phys. Z.* **1923**, *24*, 209–213.
[22] E. Zintl, A. Harder, B. Dauth, *Z. Elektrochem.* **1934**, *40*, 588–593.
[23] R. Hoppe, *Z. Kristallogr.* **1979**, *150*, 23–52.
[24] R. D. Shannon, *Acta Crystallogr., Sect. A* **1976**, *32*, 751–767.
[25] C. J. M. Rooymans, A. Rabenau, Crystal Structure and *Chemical Bonding in Inorganic Chemistry*, Elsevier-Verlag, Amsterdam, **1975**; R. Hoppe, *Angew. Chem.* **1980**, *92*, 106–121.
[26] R. Hoppe, *Angew. Chem.* **1966**, *78*, 52–63; R. Hoppe, *Adv. Fluorine Chem.* **1960**, *6*, 387; R. Hoppe, *Angew. Chem.* **1970**, *82*, 7–16; R. Hoppe, *Izvj. Jugoslav. Centr. Krist.* **1973**, *8*, 21.
[27] A. Vegas, *Acta Crystallogr., Sect. C* **1985**, *41*, 1689–1690.
[28] *X-Area*, Stoe & Cie, Darmstadt, Version 1.86, **2018**.
[29] J. Koziskova, F. Hahn, J. Richter, J. Kozisek, *Acta Chim. Slov.* **2016**, *9*, 136–140.
[30] G. M. Sheldrick, *Acta Crystallogr., Sect. A* **1990**, *46*, 467–473.
[31] G. M. Sheldrick, *SHELXS-97*, *Program for the Solution of Crystal Structures*, University of Göttingen, Germany, **1997**.
[32] G. M. Sheldrick, *SHELXL-97, Program for the Refinement of Crystal Structures*, University of Göttingen, Germany, **1997**.
[33] G. M. Sheldrick, *Acta Crystallogr., Sect. A* **2008**, *64*, 112–122.

© 2020 The Authors. Zeitschrift für anorganische und allgemeine Chemie published by Wiley-VCH GmbH

[34] R. X. Fischer, E. Tillmanns, *Acta Crystallogr., Sect. C* **1988**, *44*, 775–776.
[35] J. E. Greedan, G. J. McCarthy, *Mater. Res. Bull.* **1972**, *7*, 531–541.
[36] D. I. Galimov, R. G. Bulgakov, *Luminescence* **2019**, *34*, 127–129.
[37] W. J. Schipper, Z. A. E. P. Vroon, G. Blasse, Th. Schleid, G. Meyer, *Chem. Mater.* **1992**, *4*, 688–692.
[38] A. Diaz, D. A. Keszler, *Chem. Mater.* **1997**, *9*, 2071–2077.
[39] P. P. Larsen, *Doctoral* Thesis, University of Cologne, **2004**.
[40] Ch. Funk, J. Köhler, I. Lazar, D. Kajewski, K. Roleder, J. Nuss, A. Bussmann-Holder, H. Bamberger, J. van Slageren, D. Enseling, Th. Justel, Th. Schleid, *Cryst. Growth Des.* **2018**, *18*, 6316–6325.
[41] K. Machida, H. Hata, K. Okuno, G. Adachi, J. Shiokawa, *J. Inorg. Nucl. Chem.* **1979**, *41*, 1425–1430.
[42] K. Machida, G. Adachi, J. Shiokawa, *Acta Crystallogr., Sect. B* **1980**, *36*, 2008–2011.
[43] K. Machida, G. Adachi, Y. Moriwaki, J. Shiokawa, *Bull. Chem. Soc. Jpn.* **1981**, *54*, 1048–1051.
[44] Ch. Funk, O. Reckeweg, F. J. DiSalvo, A. Schulz, S. Klenner, R. Pöttgen, O. Janka, Th. Schleid, *J. Alloys Compd.* **2020**, *844*, 156038.
[45] J.-L. Hoslauer, Master Thesis, University of Stuttgart, **2018**.

Received: May 29, 2020
Published Online: November 12, 2020

© 2020 The Authors. Zeitschrift für anorganische und allgemeine Chemie published by Wiley-VCH GmbH